



LJMU Research Online

Zhang, G, Yao, M, Zhang, W and Zhang, W

Improved composite adaptive fault-tolerant control for dynamic positioning vehicle subject to the dead-zone nonlinearity

<http://researchonline.ljmu.ac.uk/id/eprint/25995/>

Article

Citation (please note it is advisable to refer to the publisher's version if you intend to cite from this work)

Zhang, G, Yao, M, Zhang, W and Zhang, W (2021) Improved composite adaptive fault-tolerant control for dynamic positioning vehicle subject to the dead-zone nonlinearity. IET Control Theory and Applications, 15 (16). pp. 2067-2080. ISSN 1751-8644

LJMU has developed **LJMU Research Online** for users to access the research output of the University more effectively. Copyright © and Moral Rights for the papers on this site are retained by the individual authors and/or other copyright owners. Users may download and/or print one copy of any article(s) in LJMU Research Online to facilitate their private study or for non-commercial research. You may not engage in further distribution of the material or use it for any profit-making activities or any commercial gain.

The version presented here may differ from the published version or from the version of the record. Please see the repository URL above for details on accessing the published version and note that access may require a subscription.

For more information please contact researchonline@ljmu.ac.uk

<http://researchonline.ljmu.ac.uk/>

Improved composite adaptive fault-tolerant control for dynamic positioning vehicle subject to the dead-zone nonlinearity

Guoqing Zhang¹  | Mingqi Yao¹ | Wenjun Zhang¹ | Weidong Zhang^{1,2}

¹ College of Navigation, Dalian Maritime University, Dalian 116024, People's Republic of China

² Department of Automation, Shanghai Jiao Tong University, Shanghai 200240, People's Republic of China

Correspondence

Wenjun Zhang, College of Navigation, Dalian Maritime University, No.1 Linghai Road, Dalian 116024, People's Republic of China.

Email: wenjunzhang@dmlu.edu.cn

Funding information

Science and Technology Innovation Foundation of Dalian City, Grant/Award Number: 2019J12GX026; Natural Science Foundation of Liaoning Province, Grant/Award Numbers: 20170520189, 20180520039; National Natural Science Foundation of China, Grant/Award Number: 51909018; Fundamental Research Funds for the Central Universities, Grant/Award Numbers: 3132021132, 3132021340

Abstract

In order to tackle the marine practical constraints, for example the actuator faults, the dead-zone input, an improved composite adaptive neural control algorithm is proposed for dynamic positioning vehicles in presence of the unknown external disturbances. In the algorithm, the robust neural damping technique is employed to remodel the system model uncertainty and suppress the external interference. As for the dead-zone input, the dead-zone inverse model is constructed to derive the corresponding compensating terms. That could effectively release the constraints from the actuator faults and the dead-zone non-linearity. Furthermore, for merits of the composite intelligent learning method, one designs the serial-parallel estimation model to estimate the related velocity variables. The corresponding prediction error could be applied in the design of adaptive law. That could effectively improve the accuracy of parameter estimation and facilitate the robustness of the closed-loop system. The semi-global uniformly ultimately bounded stability is guaranteed for all error signals in the closed-loop system by utilizing the Lyapunov theory. Finally, the validity of the proposed algorithm is demonstrated through the simulation experiments.

1 | INTRODUCTION

With the exploitation of ocean resources, the dynamic positioning (DP) control system has been extensively applied to various engineering ships, scientific research vessels, offshore platforms etc. Along with the growth in DP system, there is increasing concern on the working status of thrusters. Actually, the actuator faults can occur in the mechanical servo system due to its excess wear or the component aging, especially for the DP vehicle with multi actuators. That would greatly reduce the stability and positioning performance, even lead to the system crash of DP vehicle that can result in the further casualties, equipment damage and the property loss. In addition, another potential safety problem is the concomitant dead-zone input, which is particularly common in the mechanical system. The dead-zone input is with the feature of insensitivity for the small input order, which will degrade the positioning accuracy or lead to the invalidation of the conventional DP control unit. Therefore, the

investigation of the DP control, with consideration of actuator faults and the dead-zone inputs, requires more attentions to be attracted and is meaningful for the application of the theoretical design.

As the DP technology was widely used in fields of the ocean exploration, there are variety of theoretical researches both at home and abroad. For the parameter and structure uncertainty, abundant research achievements have apparently solved the problem in the DP vehicles [1–3]. It is widely known that the approximation precision of system uncertainty determines the control performance. With the increasing demand for control performance in engineering practice, it no longer meets the requires of accuracy in marine engineering only using the above fuzzy or neural networks approximators to solve the uncertainty problem. To further improve the accuracy of approximation for system uncertainties, a composite intelligent learning technology is proposed based on the serial-parallel estimation model (SPEM) in [4, 5]. Successful application of the

This is an open access article under the terms of the [Creative Commons Attribution](https://creativecommons.org/licenses/by/4.0/) License, which permits use, distribution and reproduction in any medium, provided the original work is properly cited.

© 2021 The Authors. *IET Control Theory & Applications* published by John Wiley & Sons Ltd on behalf of The Institution of Engineering and Technology

composite intelligent learning technology to the path-following control task for the underactuated cable-laying vessel, the satisfying control performance is obtained in [6]. In recent years, the controller design based on the observer is prevailing for the DP task. For example, a novel DP control approach is developed on the basis of the modified notch filter and non-linear observer in [7]. In this approach, the filtering is not related to the disturbances models and vessel model, thus the model uncertainty has not any influence for the filtering. Morishita, et al. [8] developed a modified observer backstepping controller for the DP vehicle with actuator dynamics. In this algorithm, the non-linear observer is employed to generate the state estimation variables associated with attitude and velocity under low-speed manoeuvring. And two designed gain matrices, related to error variables, are utilized to decrease the perturbation for the control signal. In [9], an output feedback adaptive control scheme is presented, where the state observer is utilized to estimate the unknown system states. And the sliding mode technique and the auxiliary system are incorporated to generate the satisfying transient performance. As the oil and gas industries developing, the DP task of individual marine vehicle has been unable to satisfy the engineering requirement. Therefore, a cooperative DP control scheme of multiple marine vehicles is proposed based upon the modular design methodology in [10]. Compared with the Lyapunov-based adaptive control design, this methodology can compensate the sudden or large external disturbances without affecting the adaptive law.

In all the aforementioned papers on dynamic positioning control, these schemes suffered from three major problems: the first one is about the dead-zone non-linearity of the actuator, that is the actuator dead-zone input is with the feature of the insensitivity for small control inputs. That is, the actuator does not act when the input signal of the actuator is small, and the actuator acts only when the input signal of the actuator reaches a certain value. Subject to the problem, a large number of studies have been achieved by researchers to address the dead-zone constraints. In [11], the dead-zone inverse model is constructed to compensate the dead-zone characteristic, and the learning law of adaptation is capable of estimating the unknown dead-zone parameters. Actually, the dead-zone parameters are always uncertain under the effect of environment factors and actuator inherent characteristics. Based on this, Liu, et al. [12] proposed a fuzzy dead-zone model, which is used to describe the uncertainty and imprecision existing in the dead-zone actuators. Therefore, that is more in line with engineering practice compared with the deterministic dead-zone model. Another dead-zone compensation methodology is developed in [13]. In this scheme, the compensator, consisting of two dynamic gain, replaces the dead-zone inverse model. This control design is more simplified since the dead-zone parameters are not required. The second one is the actuator fault, which may be frequently encountered in the practical engineering. It is caused by the excess wear or the component aging, which poses the instability of the practical system. Many alternative methods are available to solve the problem [14–16]. For example, a reliable

state feedback control strategy is developed subject to the sensor multiplicative failures in [17]. And two important factors, having an effect on the system states, are considered in this strategy, that is the premise variables of controller and sensor failures. That guarantees asymptotic stability and H_∞ performance for the closed-loop system. In [18], a discrete-time FTC method is proposed to deal with the problem of actuator faults, where the discrete-time estimator is constructed to estimate both the system states and actuator faults. And the method is able to monitor and compensate the actuator failures in real time. Different from the fault compensation approach in [17, 18], Shen, et al. [19] develop a simpler FTC algorithm to estimate and compensate the total influence of actuator failures, which tremendously relieves the computational burden.

Motivated by the above observations, a novel adaptive fault-tolerant control strategy, which is performed by using composite intelligent learning, robust neural damping and dynamic surface control (DSC) technique, is proposed for dynamic positioning vehicles with dead-zone input. Different from the existing results around the DP control, for example [1, 20, 21], the pitch ratios of thruster (for the rotatable thruster, it is the bearing angle and pitch ratio) are considered as the control input, which are all measurable variable in the engineering practice. Furthermore, the actuator faults and dead-zone non-linearity are coupled in actuators, which will pose a serious challenge to control design of the closed-loop system. The main contributions of this paper can be summarized as follows. (1) The dead-zone non-linearities and actuator faults are taken into consideration simultaneously in control design. The dead-zone non-linearity, commonly existing in the practical mechanical plant, is compensated by the adaptive smooth inverse model. In the detailed design, the corresponding adaptive law is derived to estimate the characteristic parameters for dead-zone, for example the break-points and the slopes. Aiming at the uncertainty problem of the actuator fault mode, the parameter estimation method is used to realize the fast and accurate compensation subject to the actuator faults, for example two adaptive parameters are constructed to estimate the bounds of the actuator effectiveness coefficient and bias coefficient respectively for each actuator. (2) The SPEM is constructed to improve the parameter estimation accuracy, which includes the dead-zone characteristic parameters as well as fault parameters. Furthermore, this paper releases the assumption that the control gain functions are known precisely, that is it is not required to know for the control design. That could facilitate its applicability in the engineering practice.

The remaining of this paper is organized as follows. The adaptive fault-tolerant control problem of dynamic positioning vehicle subject to the dead-zone non-linearity is introduced and some preliminaries are provided in Section 2. In Section 3, an improved composite adaptive fault-tolerant control design with dead-zone input is presented. Section 3 analyzes the stability and robustness of the closed-loop system. In Section 5, comparative experiment and experiment with actuator faults are provided to verify the effectiveness of the proposed scheme. Section 6 concludes the whole paper.

2 | PROBLEM FORMULATION AND PRELIMINARIES

Throughout the paper, $|\cdot|$ describes the absolute operator for the scalar element. $\|\cdot\|$ and $\|\cdot\|_F$ indicates the Euclidean norm and Frobenius norm of the vector, respectively. The matrix $\|\mathbf{B}\|_F^2 = \text{tr}\{\mathbf{B}^T \mathbf{B}\} = \sum_{i=1}^m \sum_{j=1}^n b_{i,j}^2$, where $\mathbf{B} = [b_{i,j}] \in \mathbb{R}^{m \times n}$ denotes a matrix. $\hat{(\cdot)}$ describes the estimation operator of (\cdot) and the estimation error $\tilde{(\cdot)} = \hat{(\cdot)} - (\cdot)$. sgn denotes the sign function, “ \cdot ” is multiplication of the element-by-element. $\text{diag}\{m_1, m_1, \dots, m_n\}$ implies a main diagonal matrix, and m_1, m_1, \dots, m_n are the diagonal elements.

2.1 | Dynamic model of marine ship

Based on the seakeeping and manoeuvring theory [22, 23], only the surge, sway, and yaw motion deserve to be discussed. Therefore, the three-degree of freedom (3-DOF) horizontal plane non-linear mathematical model of DP vehicle can be described as Equation (1).

$$\dot{\boldsymbol{\eta}} = \mathbf{J}(\boldsymbol{\psi})\mathbf{v} \quad (1)$$

$$\mathbf{M}\dot{\mathbf{v}} + \mathbf{D}_l \mathbf{v} + \mathbf{D}_n(\mathbf{v}) = \boldsymbol{\tau} + \mathbf{d}_w$$

$$\mathbf{J}(\boldsymbol{\psi}) = \begin{bmatrix} \cos \psi & -\sin \psi & 0 \\ \sin \psi & \cos \psi & 0 \\ 0 & 0 & 1 \end{bmatrix} \quad (2)$$

$$\mathbf{M} = \begin{bmatrix} m - X_{\dot{u}} & 0 & 0 \\ 0 & m - Y_{\dot{v}} & mX_G - Y_{\dot{r}} \\ 0 & mX_G - Y_{\dot{r}} & I_x - N_{\dot{r}} \end{bmatrix} \quad (3)$$

$$\mathbf{D}_l = \begin{bmatrix} -X_u & 0 & 0 \\ 0 & -Y_v & -Y_r \\ 0 & -N_v & -N_r \end{bmatrix} \quad (4)$$

$$\mathbf{D}_n(\mathbf{v}) = \begin{bmatrix} -X_{|u|u}|u|u + Y_{|v|r}|r| + Y_{\dot{r}}rr \\ -X_{\dot{u}}ur - Y_{|v|v}|v|v - Y_{|v|r}|v|r \\ (X_{\dot{u}} - Y_{\dot{v}})uv - Y_{\dot{r}}ur - N_{|v|v}|v|v - N_{|v|r}|v|r \end{bmatrix} \quad (5)$$

$$\boldsymbol{\tau} = \mathbf{T}(\boldsymbol{\beta})\boldsymbol{\kappa}(\mathbf{n})\mathbf{u}_p \quad (6)$$

In Equation (1), $\boldsymbol{\eta} = [x, y, \psi]^T \in \mathbb{R}^3$ denotes the ship attitude vector including the position coordinate (x, y) and heading angle $\psi \in [0, 2\pi]$. $\mathbf{v} = [u, v, r]^T \in \mathbb{R}^3$ is the velocity vector, where u, v, r are the velocities in the surge, sway, and yaw, respectively. $\mathbf{J}(\boldsymbol{\psi})$ indicates the rotation matrix with $\mathbf{J}^{-1}(\boldsymbol{\psi}) = \mathbf{J}^T(\boldsymbol{\psi})$, $\|\mathbf{J}(\boldsymbol{\psi})\| = 1$. Equation (3) provides with the expression of mass matrix. Furthermore, $\mathbf{D}_l \mathbf{v}$, $\mathbf{D}_n(\mathbf{v})$ are employed to describe the linear and non-linear hydrodynamic forces or moment respectively, and the specific expressions are provided in Equation (5). $X_u, X_{|u|u}, Y_v, \dots$ that could be estimated by experimental data are all the hydrodynamic force derivatives. The kinetics equation in Equation (1) contains the quadratic damping terms

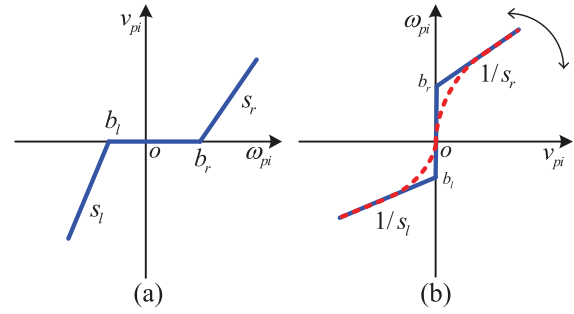


FIGURE 1 Diagram for compensating the dead-zone non-linearity: (a) the dead-zone non-linearity. (b) the smooth dead-zone inverse function

which can generate the oscillatory behaviour under low speed. Hence, the mathematical model (1) we adopted is more general for the DP vehicle.

$\boldsymbol{\tau} = [\tau_u, \tau_v, \tau_r]^T \in \mathbb{R}^3$ indicates the control input vector which contains the surge and sway control force τ_u, τ_v and the yaw control moment τ_r . $\mathbf{d}_w = [d_{wu}, d_{wv}, d_{wr}]^T \in \mathbb{R}^3$ is the external disturbance vector provided by marine environment. $\mathbf{T}(\cdot) \in \mathbb{R}^{3 \times q}$ implies the configuration matrix of thrust depending on the thrusters' physical location with the number of equivalent thrusters being q . In addition, the bearing angle of the azimuth thruster is expressed as $\boldsymbol{\beta}$. $\boldsymbol{\kappa}(\cdot) = \text{diag}\{\kappa_1(n_1), \kappa_2(n_2), \dots, \kappa_q(n_q)\} \in \mathbb{R}^{q \times q}$ is the force coefficient matrix, where $n_i, i = 1, 2, \dots, q$ denotes the propeller speed. $\mathbf{u}_p = [u_{p1}, u_{p2}, \dots, u_{pq}]^T$ with $u_{pi} = |p_i|p_i, i = 1, 2, \dots, q$. It is worth mentioning that the pitch ratio of thrusters $p_i \in [-1, 1]$ is the actual inputs for the proposed scheme.

As aforementioned, the thrusters may occur the faults due to the control signal transportation failures and other failures caused by physical factors during operation, and the dead-zone non-linearity are ubiquitous in actuators. Therefore, the fault model [24, 25] and dead-zone model [26] are described as Equations (7) and (8).

$$\mathbf{u}_p = \boldsymbol{\kappa}_p \mathbf{v}_p + \boldsymbol{\epsilon} \quad (7)$$

$$v_{pi} = \text{DZ}(\omega_{pi}) = \begin{cases} s_r(\omega_{pi} - b_r) & \omega_{pi} \geq b_r \\ 0 & b_l < \omega_{pi} < b_r \\ s_l(\omega_{pi} - b_l) & \omega_{pi} \leq b_l \end{cases} \quad (8)$$

where $\boldsymbol{\kappa}_p = \text{diag}\{\kappa_{p1}, \kappa_{p2}, \dots, \kappa_{pq}\} \in \mathbb{R}^{q \times q}$ is the actuator effectiveness coefficient matrix with $0 \leq \kappa_{pi} \leq 1, i = 1, 2, \dots, q$, $\mathbf{v}_p = [v_{p1}, v_{p2}, \dots, v_{pq}]^T \in \mathbb{R}^q$ be a vector indicating actuator dead-zone output, \mathbf{u}_p is actuator output vector, $\boldsymbol{\epsilon} = [\epsilon_1, \epsilon_2, \dots, \epsilon_q]^T \in \mathbb{R}^q$ denotes the bias fault matrix. For the dead-zone model, $b_l \leq 0, b_r \geq 0$ are the break-points with $|b_l| \neq |b_r|, s_r > 0, s_l > 0$ denote the slopes with $|s_r| \neq |s_l|$. The graphical representation of the dead-zone is shown in Figure 1(a). v_{pi} is the dead-zone output of i th actuator and ω_{pi} denotes the dead-zone input of the i th actuator. As for the fault model (7), there are four fault modes, as explained in the following.

(1) $\kappa_{pi} = 1$ and $\epsilon_i = 0$. This indicates that the i th actuator is working normally.

(2) $0 < k_{pi} < 1$ and $\epsilon_i = 0$. This is a sign that the partial loss of effectiveness (PLOE) is being experienced for the i th actuator.

(3) $k_{pi} = 1$ and $\epsilon_i \neq 0$. This is indicative of the bias fault from the i th actuator.

(4) $k_{pi} = 0$. This means that the i th actuator is suffering the total loss of effectiveness (TLOE), that is $u_{pi} = \epsilon_i$.

Assumption 1. The mass matrix \mathbf{M} is positive-definite and invertible, following [27].

Assumption 2. [6, 27] \mathbf{d}_w is the bounded disturbance vector, that is there exists a positive constant vector $\bar{\mathbf{d}}_w = [\bar{d}_{wu}, \bar{d}_{wv}, \bar{d}_{wr}]^T$, such that $d_{wu} \leq \bar{d}_{wu}$, $d_{wv} \leq \bar{d}_{wv}$, $d_{wr} \leq \bar{d}_{wr}$. And $\bar{\mathbf{d}}_w$ is unknown for the control design.

Assumption 3. [28] The dead-zone parameters satisfy $s_r \geq s_{r0}$, $s_j \geq s_{j0}$, where s_{r0} , s_{j0} are all small positive constants.

Remark 1. In practice, the DP vehicle hull is port-starboard symmetrical and approximately fore-aft symmetrical. Therefore, Assumption 1 is automatically satisfied in the marine practice. Assumption 2 is a common precondition for ship motion control in the existing literatures. As for the dead-zone actuator, it is with the feature of the insensitivity for small control input signals. But it will be responseless for arbitrary control input signals with the dead-zone parameters $s_r = s_j = 0$, for example it is equivalent to the TLOE fault at the moment. That is meaningless and insignificant. Therefore, Assumption 3 is necessary and reasonable in practical applications.

Remark 2. In marine engineering, the force coefficient is a constant with $0 < \underline{\kappa}_i \leq \kappa_i(u_i) \leq \bar{\kappa}_i$, $i = 1, 2, \dots, q$, where $\underline{\kappa}_i$ and $\bar{\kappa}_i$ are both unknown.

Actually, actual control inputs consist of the pitch ratio and bearing angle of the rotatable thruster. To solve the thrust allocation problem, the rotatable actuator could be extended as two forces in horizon and vertical for the DP vehicle. Taking a marine vessel with two main propellers and one rotatable thruster as an example, the extending operation is provided in Equation (9).

$$\begin{aligned} \boldsymbol{\tau} &= \underbrace{\begin{bmatrix} 1 & 1 & \cos(\beta_3) \\ 0 & 0 & \sin(\beta_3) \\ l_{y1} & -l_{y2} & l_{x3} \sin(\beta_3) \end{bmatrix}}_{\text{The actual matrix } T(\beta)} \begin{bmatrix} \kappa_1 & 0 & 0 \\ 0 & \kappa_2 & 0 \\ 0 & 0 & \kappa_3 \end{bmatrix} \begin{bmatrix} u_1 \\ u_2 \\ u_3 \end{bmatrix} \\ &= \underbrace{\begin{bmatrix} 1 & 1 & 1 & 0 \\ 0 & 0 & 0 & 1 \\ l_{y1} & -l_{y2} & 0 & l_{x3} \end{bmatrix}}_{\text{The extended matrix}} \begin{bmatrix} \kappa_1 & 0 & 0 & 0 \\ 0 & \kappa_2 & 0 & 0 \\ 0 & 0 & \kappa_3 & 0 \\ 0 & 0 & 0 & \kappa_3 \end{bmatrix} \begin{bmatrix} u_1 \\ u_2 \\ u_{3x} \\ u_{3y} \end{bmatrix} \end{aligned} \quad (9)$$

Besides, the equivalent control inputs $u_{3x} = u_3 \cos(\beta_3)$, $u_{3y} = u_3 \sin(\beta_3)$. The actual control input p_3 and β_3 could be derived based on Equation (10).

$$u_3 = |p_3| p_3 = \sqrt{u_{3x}^2 + u_{3y}^2}, \beta_3 = \arctan(u_{3x}, u_{3y}) \quad (10)$$

The marine practical constraints we took into account include the dead-zone input, gain uncertainties, actuator faults and unmodelled dynamics. The control objective of this paper is to develop an improved composite adaptive fault-tolerant controller (pitch ratio and bearing angle are used as the control input) to deal with the above mentioned obstructions, such that the dynamic positioning vehicle is maintained exactly in the pre-set position with the desired attitude.

2.2 | NNs-based function approximation

The radical basic function (RBF) neural networks (NNs) are employed to address the problem of system uncertainty with its excellent capability of function approximation. And the robust neural damping term is further derived to improve the robustness and the stability for the closed-loop system, and it is able to perform the concise form and requires smaller computational space in practice.

Lemma 1. [6, 27] For any given continuous function $f(\mathbf{x})$ with $f(\mathbf{0}) = 0$, $f(\mathbf{x})$ can be approximated as Equation (11) by employing RBF NNs approximation and the continuous function separation technique.

$$f(\mathbf{x}) = \mathcal{S}(\mathbf{x})\mathbf{A}\mathbf{x} + \boldsymbol{\varepsilon}_x \quad (11)$$

where $\mathbf{x} \in \mathbb{B}_x$ denotes the input vector, and \mathbb{B}_x is a compact set in \mathbb{R}^n . $\mathcal{S}(\mathbf{x}) = [s_1(\mathbf{x}), s_2(\mathbf{x}), \dots, s_l(\mathbf{x})]$ is a RBF vector with the form of Gaussian function (12), and $\boldsymbol{\varepsilon}_x$ is the approximation error with its upper bound being $\bar{\boldsymbol{\varepsilon}}_x$.

$$s_i(\mathbf{x}) = \frac{1}{\sqrt{2\pi}\varrho_i} \exp\left(-\frac{(\mathbf{x} - \boldsymbol{\mu}_i)^T(\mathbf{x} - \boldsymbol{\mu}_i)}{2\varrho_i^2}\right) \quad (12)$$

In Equation (12), $\boldsymbol{\mu}_i = [\mu_{i1}, \mu_{i2}, \dots, \mu_{in}]$ indicates the centre of the receptive field and ϱ_i is the width of the Gaussian function, n denotes the dimension number of the state vector \mathbf{x} , $i = 1, 2, \dots, l$, l is the node number of NNs, and

$$\mathbf{A} = \begin{bmatrix} \omega_{11} & \omega_{12} & \cdots & \omega_{1n} \\ \omega_{21} & \omega_{22} & \cdots & \omega_{2n} \\ \vdots & \vdots & \ddots & \vdots \\ \omega_{l1} & \omega_{l2} & \cdots & \omega_{ln} \end{bmatrix}$$

is the weight matrix.

3 | IMPROVED COMPOSITE ADAPTIVE FAULT-TOLERANT CONTROLLER

3.1 | Dead-zone inverse model

To eliminate the dead-zone effect, the dead-zone inverse model in Equation (13) is introduced for the control design, which is shown in Figure 1(b),

$$\omega_{pi} = \frac{v_{pi} + s_r b_r}{s_r} \Phi_r(v_{pi}) + \frac{v_{pi} + s_l b_l}{s_l} \Phi_l(v_{pi}) \quad (13)$$

where $\Phi_r(v_{pi})$ and $\Phi_l(v_{pi})$ are smooth continuous functions with $j = 1, 2, \dots, q$, and their expressions could be described as Equation (14).

$$\Phi_r(v_{pi}) = \frac{\frac{v_{pi}}{e^{a_0}}}{e^{-\frac{v_{pi}}{a_0}} + e^{a_0}}, \quad \Phi_l(v_{pi}) = \frac{-\frac{v_{pi}}{e^{a_0}}}{e^{-\frac{v_{pi}}{a_0}} + e^{a_0}} \quad (14)$$

In Equation (14), $a_0 > 0$ denotes a parameter defined by designer. To facilitate the illustration, the dead-zone is parameterized as Equation (15),

$$v_{pi} = -\vartheta_i^T \varphi_i, \quad i = 1, 2, \dots, q \quad (15)$$

where

$$\vartheta_i^T = [s_r, s_r b_r, s_l, s_l b_l] \quad (16)$$

$$\varphi_i^T = [-\epsilon_r \omega_{pi}, \epsilon_r, -\epsilon_l \omega_{pi}, \epsilon_l] \quad (17)$$

$$\epsilon_r = \begin{cases} 1, & v_{pi} > 0 \\ 0, & \text{others} \end{cases}, \quad \epsilon_l = \begin{cases} 1, & v_{pi} < 0 \\ 0, & \text{others} \end{cases} \quad (18)$$

Since ϑ_i is unknown and φ_i is unavailable, v_{pi} could be designed as Equation (19),

$$v_{di} = -\hat{\vartheta}_i^T \hat{\varphi}_i, \quad i = 1, 2, \dots, q \quad (19)$$

where $\hat{\vartheta}_i$ is the estimation of ϑ_i .

$$\hat{\vartheta}_i^T = [\hat{s}_r, \hat{s}_r \hat{b}_r, \hat{s}_l, \hat{s}_l \hat{b}_l] \quad (20)$$

$$\hat{\varphi}_i^T = [-\Phi_r(\omega_{pi}) \omega_{pi}, \Phi_r(\omega_{pi}), -\Phi_l(\omega_{pi}) \omega_{pi}, \Phi_l(\omega_{pi})] \quad (21)$$

Hence the i th actuator input ω_{pi} could be derived as Equation (22).

$$\omega_{pi} = \frac{v_{di} + \hat{s}_r \hat{b}_r}{\hat{s}_r} \Phi_r(v_{di}) + \frac{v_{di} + \hat{s}_l \hat{b}_l}{\hat{s}_l} \Phi_l(v_{di}) \quad (22)$$

The compensation error is given in Equation (23),

$$v_{pi} - v_{di} = \tilde{\vartheta}_i^T \hat{\varphi}_i + \delta_i \quad (23)$$

where $\tilde{\vartheta}_i = \hat{\vartheta}_i - \vartheta_i$, $\delta_i = \vartheta_i^T (\varphi_i - \hat{\varphi}_i)$. As described in [26], the upper bound of δ_i could be derived as Equation (24).

$$\begin{aligned} |\delta_i| &= \left| \vartheta_i^T (\varphi_i - \hat{\varphi}_i) \right| \\ &\leq \begin{cases} \frac{1}{2} e^{-1} |s_r - s_l| a_0 + \frac{|s_r b_r - s_l b_l|}{e^{2b_r/a_0} + 1}, & \omega_{pi} \geq b_r \\ \max\{s_r, s_l\} |b_r - b_l|, & b_l < \omega_{pi} < b_r \\ \frac{1}{2} e^{-1} |s_r - s_l| a_0 + \frac{|s_r b_r - s_l b_l|}{e^{-2b_l/a_0} + 1}, & \omega_{pi} \leq b_l \end{cases} \quad (24) \\ &= \bar{\delta}_i \end{aligned}$$

It is noteworthy that $\bar{\delta}_i$ is bounded for all $t \geq 0$ and $\bar{\delta}_i$ asymptotically converges 0 with $\hat{\vartheta}_i \rightarrow \vartheta_i$ and $a_0 \rightarrow 0$.

3.2 | Control design

Step 1: Define the error vector $\eta_e = \eta_d - \eta$, $\eta_d \in \mathbb{R}^3$ is the desired attitude vector with its elements being constant. Then $\dot{\eta}_e$ could be expressed as Equation (25).

$$\dot{\eta}_e = \dot{\eta}_d - J(\psi)v \quad (25)$$

The virtual control α_v is designed as Equation (26), where k_η is the designed diagonal matrix with its diagonal elements being positive.

$$\alpha_v = J^{-1}(\psi) k_\eta \eta_e \quad (26)$$

To avoid the explosion of complexity, one employ the dynamic surface control (DSC) technique here, that is let the term α_v pass through a first-order filter.

$$\varrho_v \dot{\beta}_v + \beta_v = \alpha_v, \quad \beta_v(0) = \alpha_v(0) \quad (27)$$

In Equation (27), $\varrho_v = \text{diag}\{\varrho_u, \varrho_v, \varrho_r\}$ is the time constant matrix and β_v indicates the reference signal for the velocity vector v . Define $v_e = \beta_v - v$ and $\chi_v = \alpha_v - \beta_v$, the derivative of χ_v could be derived as Equation (28),

$$\begin{aligned} \dot{\chi}_v &= -\dot{\beta}_v + \dot{\alpha}_v \\ &= -\varrho_v^{-1} \chi_v + R_v(\eta_e, \dot{\eta}_e, \psi, r) \\ &= \sum_{i=u,v,r} (-\varrho_i^{-1} \chi_i + R_i(\eta_e, \dot{\eta}_e, \psi, r)) \end{aligned} \quad (28)$$

where $\mathbf{R}_v(\cdot) = [R_u(\cdot), R_v(\cdot), R_r(\cdot)]^T$ denotes a continuous functions vector, and its elements satisfy the condition that $|R_u(\cdot)| \leq \bar{R}_u$, $|R_v(\cdot)| \leq \bar{R}_v$, $|R_r(\cdot)| \leq \bar{R}_r$ with $\bar{R}_u, \bar{R}_v, \bar{R}_r$ being the unknown positive constants. The error vector $\boldsymbol{\eta}_e$ could be rewritten as Equation (29).

$$\begin{aligned}\dot{\boldsymbol{\eta}}_e &= \dot{\boldsymbol{\eta}}_d - \mathbf{J}(\boldsymbol{\psi})(\boldsymbol{\alpha}_v - \boldsymbol{\chi}_v - \mathbf{v}_e) \\ &= -\mathbf{k}_\eta \boldsymbol{\eta}_e + \mathbf{J}(\boldsymbol{\psi})\boldsymbol{\chi}_v + \mathbf{J}(\boldsymbol{\psi})\mathbf{v}_e\end{aligned}\quad (29)$$

Step 2: According to Equation (1), one can obtain Equation (30),

$$\dot{\mathbf{v}}_e = \dot{\boldsymbol{\beta}}_v - \mathbf{M}^{-1}[-\mathbf{D}_l \mathbf{v} - \mathbf{D}_n(\mathbf{v}) + \mathbf{T}(\boldsymbol{\beta})\boldsymbol{\kappa}(\mathbf{n})\mathbf{u}_p + \mathbf{d}_w]\quad (30)$$

The RBF NNs is employed to solve the system uncertainty $\mathbf{D}_l \mathbf{v} + \mathbf{D}_n(\mathbf{v})$ by fusion of lemma 1.

$$\begin{aligned}\mathbf{F}_{mn}(\mathbf{v}) &= \mathcal{S}_{\bar{v}}(\mathbf{v})\mathbf{A}_{\bar{v}}\mathbf{v} + \boldsymbol{\varepsilon}_{\bar{v}} \\ &= \begin{bmatrix} \mathcal{S}_u(\mathbf{v}) & 0 & 0 \\ 0 & \mathcal{S}_v(\mathbf{v}) & 0 \\ 0 & 0 & \mathcal{S}_r(\mathbf{v}) \end{bmatrix} \begin{bmatrix} \mathbf{A}_u \\ \mathbf{A}_v \\ \mathbf{A}_r \end{bmatrix} \begin{bmatrix} \mathbf{u} \\ \mathbf{v} \\ \mathbf{r} \end{bmatrix} + \begin{bmatrix} \boldsymbol{\varepsilon}_u \\ \boldsymbol{\varepsilon}_v \\ \boldsymbol{\varepsilon}_r \end{bmatrix} \\ &= \mathcal{S}_{\bar{v}}(\mathbf{v})\mathbf{A}_{\bar{v}}\boldsymbol{\beta}_v - \mathcal{S}_{\bar{v}}(\mathbf{v})\mathbf{A}_{\bar{v}}\mathbf{v}_e + \boldsymbol{\varepsilon}_{\bar{v}} \\ &= \mathcal{S}_{\bar{v}}(\mathbf{v})\mathbf{A}_{\bar{v}}\boldsymbol{\beta}_v - b_v \mathcal{S}_v(\mathbf{v})\boldsymbol{\omega}_v + \boldsymbol{\varepsilon}_{\bar{v}}\end{aligned}\quad (31)$$

In Equation (31), $\mathbf{F}_{mn}(\mathbf{v}) = [f_{mu}(\mathbf{v}), f_{mv}(\mathbf{v}), f_{mr}(\mathbf{v})]^T \in \mathbb{R}^3$ contains three RBF NNs, which are chosen to deal with the uncertainty for the u , v , r subsystems. $\mathcal{S}_{\bar{v}}(\mathbf{v}) \in \mathbb{R}^{3 \times 3l}$, $\mathbf{A}_{\bar{v}} \in \mathbb{R}^{3l \times 3}$. In fact, $\mathcal{S}_u(\mathbf{v}) = \mathcal{S}_v(\mathbf{v}) = \mathcal{S}_r(\mathbf{v})$ since they are with the same input vector \mathbf{v} . $\mathbf{A}_{\bar{v}} = [\mathbf{A}_u, \mathbf{A}_v, \mathbf{A}_r]^T \in \mathbb{R}^3$, $\boldsymbol{\varepsilon}_{\bar{v}} = [\boldsymbol{\varepsilon}_u, \boldsymbol{\varepsilon}_v, \boldsymbol{\varepsilon}_r]^T \in \mathbb{R}^3$, and $\bar{\boldsymbol{\varepsilon}}_{\bar{v}}$ is the upper bound vector of $\boldsymbol{\varepsilon}_{\bar{v}}$. In addition, $b_v = \|\mathbf{A}_{\bar{v}}\|_F$, $\mathbf{A}_{\bar{v}}^{\#} = \mathbf{A}_{\bar{v}} / \|\mathbf{A}_{\bar{v}}\|_F$, thus one can obtain $\boldsymbol{\omega}_v = \mathbf{A}_{\bar{v}}^{\#} \mathbf{v}_e$ and $b_v \boldsymbol{\omega}_v = \mathbf{A}_{\bar{v}} \mathbf{v}_e$. Then one can construct the robust neural damping term $\boldsymbol{\zeta}$, as shown in Equation (32),

$$\begin{aligned}\boldsymbol{\zeta} &= \mathcal{S}_{\bar{v}}(\mathbf{v})\mathbf{A}_{\bar{v}}\boldsymbol{\beta}_v + \boldsymbol{\varepsilon}_{\bar{v}} - \mathbf{d}_w \\ &\leq \mathcal{S}_{\bar{v}}(\mathbf{v})\mathbf{A}_{\bar{v}}\boldsymbol{\beta}_v + \bar{\boldsymbol{\varepsilon}}_{\bar{v}} - \bar{\mathbf{d}}_w \\ &\leq \rho_v \boldsymbol{\phi}_v(\cdot)\end{aligned}\quad (32)$$

where $\boldsymbol{\phi}_v(\cdot) = 1 + \|\mathcal{S}_{\bar{v}}(\mathbf{v})\| \|\boldsymbol{\beta}_v\|$, $\rho_v = \max\{\|\mathbf{A}_{\bar{v}}\|_F, \|\bar{\mathbf{d}}_w\| + \|\bar{\boldsymbol{\varepsilon}}_{\bar{v}}\|\}$. Equation (33) could be obtained on the basis of the Young's inequality.

$$\begin{aligned}& \mathbf{v}_e^T \boldsymbol{\zeta} - b_v \mathbf{v}_e^T \mathcal{S}_{\bar{v}}(\mathbf{v})\boldsymbol{\omega}_v \\ & \leq \frac{\boldsymbol{\phi}_v^2 \mathbf{v}_e^T \mathbf{k}_{mn} \mathbf{v}_e}{4} + \frac{\rho_v^2}{\lambda_{\min}\{\mathbf{k}_{mn}\}} + \frac{\|\mathcal{S}_{\bar{v}}(\mathbf{v})\|_F^2 \mathbf{v}_e^T \mathbf{k}_{mn} \mathbf{v}_e}{4} \\ & \quad + \frac{b_v^2 \boldsymbol{\omega}_v^T \boldsymbol{\omega}_v}{\lambda_{\min}\{\mathbf{k}_{mn}\}} \\ & = \Phi_v(\cdot) \mathbf{v}_e^T \mathbf{k}_{mn} \mathbf{v}_e + \frac{\rho_v^2}{\lambda_{\min}\{\mathbf{k}_{mn}\}} + \frac{b_v^2 \boldsymbol{\omega}_v^T \boldsymbol{\omega}_v}{\lambda_{\min}\{\mathbf{k}_{mn}\}}\end{aligned}\quad (33)$$

In Equation (33), $\Phi_v(\cdot) = (1/4)(\boldsymbol{\phi}_v^2 + \|\mathcal{S}_{\bar{v}}(\mathbf{v})\|_F^2)$, \mathbf{k}_{mn} is the designed positive diagonal parameter matrix.

On the basis of above analysis, the error dynamic (30) can be rewritten as Equation (34).

$$\dot{\mathbf{v}}_e = \mathbf{M}^{-1}(\mathbf{M}\dot{\boldsymbol{\beta}}_v + \boldsymbol{\zeta} - b_v \mathcal{S}_{\bar{v}}(\mathbf{v})\boldsymbol{\omega}_v - \mathbf{T}(\boldsymbol{\beta})\boldsymbol{\kappa}(\mathbf{n})\mathbf{u}_p)\quad (34)$$

By incorporating the actuator fault model (7), the dead-zone model (8), dead-zone inverse model (13) and error dynamics (34), it yields Equation (35),

$$\begin{aligned}\dot{\mathbf{v}}_e &= \mathbf{M}^{-1}(\mathbf{M}\dot{\boldsymbol{\beta}}_v + \boldsymbol{\zeta} - b_v \mathcal{S}_{\bar{v}}(\mathbf{v})\boldsymbol{\omega}_v - \mathbf{T}(\boldsymbol{\beta})\boldsymbol{\kappa}(\mathbf{n})\boldsymbol{\varepsilon} \\ & \quad - \mathbf{T}(\boldsymbol{\beta})\boldsymbol{\kappa}(\mathbf{n})\mathbf{k}_p(\mathbf{v}_p - \mathbf{v}_d + \mathbf{v}_d)) \\ & = \mathbf{M}^{-1}(\mathbf{M}\dot{\boldsymbol{\beta}}_v + \boldsymbol{\zeta} - b_v \mathcal{S}_{\bar{v}}(\mathbf{v})\boldsymbol{\omega}_v - \mathbf{T}(\boldsymbol{\beta})\boldsymbol{\kappa}(\mathbf{n})\mathbf{k}_p \mathbf{A} \\ & \quad - \mathbf{T}(\boldsymbol{\beta})\boldsymbol{\kappa}(\mathbf{n})\mathbf{k}_p \boldsymbol{\delta} - \mathbf{T}(\boldsymbol{\beta})\boldsymbol{\kappa}(\mathbf{n})\mathbf{k}_p \mathbf{v}_d - \mathbf{T}(\boldsymbol{\beta})\boldsymbol{\kappa}(\mathbf{n})\boldsymbol{\varepsilon})\end{aligned}\quad (35)$$

where $\mathbf{v}_p - \mathbf{v}_d = \mathbf{A} + \boldsymbol{\delta}$ by virtue of Equation (23), and $\mathbf{v}_d = [v_{d1}, v_{d2}, \dots, v_{dq}]^T$, $\boldsymbol{\delta} = [\delta_1, \delta_2, \dots, \delta_q]^T$, $\mathbf{A} = [\hat{\boldsymbol{\theta}}_1^T \hat{\boldsymbol{\phi}}_1, \hat{\boldsymbol{\theta}}_2^T \hat{\boldsymbol{\phi}}_2, \dots, \hat{\boldsymbol{\theta}}_q^T \hat{\boldsymbol{\phi}}_q]^T$.

In the practice engineering, the thruster force coefficient $\kappa_i(\cdot)$ and actuator fault parameters k_{pi}, ε_i are unknown and may bring about the system gain uncertainty. To ascertain these terms, one can define $\mathbf{g}_p = \text{diag}\{g_{p1}, g_{p2}, \dots, g_{pq}\} = \boldsymbol{\kappa}(\mathbf{n})\mathbf{k}_p$, $\boldsymbol{\omega}_p = -\boldsymbol{\kappa}(\mathbf{n})(\mathbf{k}_p \boldsymbol{\delta} + \boldsymbol{\varepsilon})$, then it can be obtained that $\boldsymbol{\lambda} = \text{diag}\{\lambda_1, \lambda_2, \dots, \lambda_q\} = \text{diag}\{1/g_{p1}, 1/g_{p2}, \dots, 1/g_{pq}\}$, $\boldsymbol{\theta} = \text{diag}\{\theta_1, \theta_2, \dots, \theta_q\} = \boldsymbol{\lambda} \sup \|\boldsymbol{\omega}_p\| \boldsymbol{\xi}$, where $\boldsymbol{\xi} = [1, 1, \dots, 1]^T$. The adaptive parameters $\hat{\lambda}_i, \hat{\theta}_i$ are designed to estimate λ_i, θ_i . They are updated online to compensate the gain uncertainties, actuator faults and dead-zone constraints. According to the above analysis, one can obtain Equation (36).

$$\begin{aligned}\dot{\mathbf{v}}_e &= \mathbf{M}^{-1}(\mathbf{M}\dot{\boldsymbol{\beta}}_v + \boldsymbol{\zeta} - b_v \mathcal{S}_{\bar{v}}(\mathbf{v})\boldsymbol{\omega}_v - \mathbf{T}(\boldsymbol{\beta})\mathbf{g}_p \mathbf{A} \\ & \quad - \mathbf{T}(\boldsymbol{\beta})\mathbf{g}_p \mathbf{v}_d + \mathbf{T}(\boldsymbol{\beta})\boldsymbol{\omega}_p)\end{aligned}\quad (36)$$

The immediate control variable $\boldsymbol{\alpha}_u = [\alpha_{up}, \alpha_{vp}, \alpha_{rp}]^T$ are designed as Equation (37) for the thrust term $\mathbf{T}(\boldsymbol{\beta})\boldsymbol{\kappa}(\mathbf{n})\mathbf{v}_d$. The actual control law for the dead-zone input $\boldsymbol{\omega}_p$ is derived as Equation (38),

$$\boldsymbol{\alpha}_u = \mathbf{k}_v \mathbf{v}_e + \dot{\boldsymbol{\beta}}_v + \Phi_v(\cdot) \mathbf{k}_{mn} \mathbf{v}_e + \mathbf{J}^T(\boldsymbol{\psi}) \boldsymbol{\eta}_e\quad (37)$$

$$\mathbf{p} = \text{sgn}(\boldsymbol{\omega}_p) * \sqrt{|\boldsymbol{\omega}_p|}$$

$$\mathbf{v}_d = \text{diag}\{\hat{\lambda}_1, \hat{\lambda}_2, \dots, \hat{\lambda}_q\} \mathbf{T}^\dagger(\boldsymbol{\beta}) \boldsymbol{\alpha}_u - \text{diag}\{\hat{\theta}_1, \hat{\theta}_2, \dots, \hat{\theta}_q\} \boldsymbol{\Theta}\quad (38)$$

where $\boldsymbol{\Theta} = [\tanh(\hat{\theta}_1(\mathbf{v}_e + \boldsymbol{\gamma}_{\hat{\theta}_1} \boldsymbol{\zeta})^T \mathbf{T}_1(\cdot)/\varepsilon), \dots, \tanh(\hat{\theta}_q(\mathbf{v}_e + \boldsymbol{\gamma}_{\hat{\theta}_q} \boldsymbol{\zeta})^T \mathbf{T}_q(\cdot)/\varepsilon)]^T$ with $\varepsilon > 0$, $\mathbf{T}^\dagger(\boldsymbol{\beta})$ is the pseudo inverse of $\mathbf{T}(\boldsymbol{\beta})$, $\mathbf{T}_i(\cdot)$ denotes the i th column of the matrix $\mathbf{T}(\cdot)$, $\boldsymbol{\omega}_p = [\omega_{p1}, \omega_{p2}, \dots, \omega_{pq}]^T \in \mathbb{R}^q$.

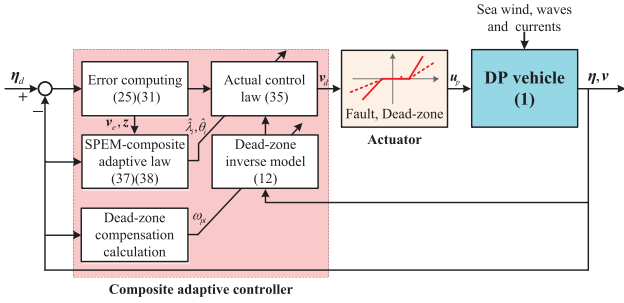


FIGURE 2 The conceptual signal flow diagram for the proposed scheme

To further improve parameter estimation accuracy, one employs the SPEM (39) to estimate the velocity variable. The SPEM is designed on the basis of Equation (34) and the corresponding prediction error is $\mathbf{z} = \hat{\mathbf{v}} - \mathbf{v}$, where $\boldsymbol{\varsigma}$ is the designed diagonal parameter matrix.

$$\dot{\hat{\mathbf{v}}} = \boldsymbol{\alpha}_u - \Phi_v(\cdot) \mathbf{k}_{vm} \mathbf{v}_e - \boldsymbol{\varsigma} \mathbf{z} \quad (39)$$

The composite adaptive laws are presented as Equations (40)–(42). They are with the concise form and robustness, which is more in accordance with requirements for the practice engineering,

$$\dot{\hat{\boldsymbol{\theta}}}_i = \boldsymbol{\Gamma}_{\theta_i} \left[\left(\mathbf{v}_e + \boldsymbol{\gamma}_{\mathbf{z}} \mathbf{z} \right)^T \mathbf{T}_i(\cdot) \hat{\boldsymbol{\phi}}_i - \sigma_{\theta_i} (\hat{\boldsymbol{\theta}}_i - \hat{\boldsymbol{\theta}}_i(0)) \right] \quad (40)$$

$$\begin{aligned} \dot{\hat{\lambda}}_i = & \boldsymbol{\Gamma}_{\lambda_i} \left[\sum_{k=u,v,r} \sum_{j=u,v,r} \mathbf{T}_{ij}^T(\cdot) \mathbf{T}_{ki}(\cdot) (\mathbf{k}_e + \boldsymbol{\gamma}_{\mathbf{z}} \mathbf{k}_{\mathbf{z}}) \boldsymbol{\alpha}_{jp} \right. \\ & \left. - \sigma_{\lambda_i} (\hat{\lambda}_i - \hat{\lambda}_i(0)) \right] \end{aligned} \quad (41)$$

$$\dot{\hat{\boldsymbol{\theta}}}_i = \boldsymbol{\Gamma}_{\theta_i} \left[\left(\mathbf{v}_e + \boldsymbol{\gamma}_{\mathbf{z}} \mathbf{z} \right)^T \mathbf{T}_i(\cdot) - \sigma_{\theta_i} (\hat{\boldsymbol{\theta}}_i - \hat{\boldsymbol{\theta}}_i(0)) \right] \quad (42)$$

where $\boldsymbol{\Gamma}_{\theta_i}$ is the positive-definite matrix, and $\boldsymbol{\Gamma}_{\lambda_i}$, $\boldsymbol{\Gamma}_{\theta_i}$, σ_{θ_i} , σ_{λ_i} , σ_{θ_i} ; all are the design parameters, $\boldsymbol{\gamma}_{\mathbf{z}} = \text{diag}\{\boldsymbol{\gamma}_{\mathbf{z}u}, \boldsymbol{\gamma}_{\mathbf{z}v}, \boldsymbol{\gamma}_{\mathbf{z}r}\}$ is the designed parameter matrices.

To sum up, the aforementioned improved composite adaptive fault-tolerant controller is designed by fusion of the composite intelligent learning technique, fault estimation method and dead-zone inverse compensation strategy. The conceptual signal flow diagram of the proposed controller is shown in Figure 2.

Remark 3. The proposed improved composite adaptive control scheme overcomes one major obstacle for the application of composite neural learning technology, for example it would relax the strict assumption in [28] that the control gain functions could be known precisely. The aim of this paper is to combine the control gain with actuator fault parameters and they are handled as adaptive updating law. The prediction error \mathbf{z} between the system state and its estimation value is employed to construct the composite adaptive laws (40)–(42). By combining with the prediction error, the accuracy of parameter estimation

is enhanced significantly. As for the composite law (40), the prediction error improves the estimation accuracy for the unknown dead-zone parameters, which could compensate the dead-zone non-linearities more precisely. Only two gain and fault related adaptive laws (41),(42) are required to compensate the perturbation caused by gain uncertainty and actuator failures. And the compensation accuracy is improved markedly because of the existence of the prediction error. Hence the proposed algorithm has a wider range of applicability in the marine industry.

4 | STABILITY ANALYSIS

In this section, the stability analysis is stated as follows.

Theorem 1. Consider the closed-loop system containing the DP vehicle model (1) holding assumption 1-3, the control variable (26)(37), the composite dead-zone update law (40), and composite adaptive law (41)(42). The initial condition satisfies $\boldsymbol{\eta}_e(0)^T \boldsymbol{\eta}_e(0) + \mathbf{v}_e(0)^T \mathbf{v}_e(0) + \boldsymbol{\chi}_v(0)^T \boldsymbol{\chi}_v(0) + \mathbf{z}(0)^T \mathbf{z}(0) + \sum_{i=1}^q \hat{\boldsymbol{\theta}}_i(0)^T \hat{\boldsymbol{\theta}}_i(0) + \sum_{i=1}^q \tilde{\lambda}_i^2(0) + \sum_{i=1}^q \hat{\boldsymbol{\theta}}_i^2(0) \leq \Delta$ with any $\Delta > 0$, $i = 1, 2, \dots, q$. All the signals are semi-global uniformly ultimately bounded (SGUUB) by tuning the parameters \mathbf{k}_{η} , \mathbf{k}_v , \mathbf{k}_{vm} , $\boldsymbol{\rho}_v$, $\boldsymbol{\varsigma}$, $\boldsymbol{\Gamma}_{\theta_i}$, σ_{θ_i} , $\boldsymbol{\gamma}_{\mathbf{z}}$, $\boldsymbol{\Gamma}_{\lambda_i}$, $\boldsymbol{\Gamma}_{\theta_i}$, σ_{λ_i} , σ_{θ_i} approximately.

Proof. On the basis of the control design process, the Lyapunov function candidate could be constructed as Equation (43).

$$\begin{aligned} \mathcal{V} = & \frac{1}{2} \boldsymbol{\eta}_e^T \boldsymbol{\eta}_e + \frac{1}{2} \mathbf{v}_e^T \mathbf{M} \mathbf{v}_e + \frac{1}{2} \boldsymbol{\chi}_v^T \boldsymbol{\chi}_v + \frac{1}{2} \mathbf{z}^T \boldsymbol{\gamma}_{\mathbf{z}} \mathbf{z} \\ & + \frac{1}{2} \sum_{i=1}^q g_{pi} \hat{\boldsymbol{\theta}}_i^T \boldsymbol{\Gamma}_{\theta_i}^{-1} \hat{\boldsymbol{\theta}}_i + \frac{1}{2} \sum_{i=1}^q \frac{g_{pi} \tilde{\lambda}_i^2}{\boldsymbol{\Gamma}_{\lambda_i}} + \frac{1}{2} \sum_{i=1}^q \frac{g_{pi} \hat{\boldsymbol{\theta}}_i^2}{\boldsymbol{\Gamma}_{\theta_i}} \end{aligned} \quad (43)$$

Then the time derivative of \mathcal{V} can be presented as Equation (44).

$$\begin{aligned} \dot{\mathcal{V}} = & \boldsymbol{\eta}_e^T \dot{\boldsymbol{\eta}}_e + \mathbf{v}_e^T \mathbf{M} \dot{\mathbf{v}}_e + \boldsymbol{\chi}_v^T \dot{\boldsymbol{\chi}}_v + \mathbf{z}^T \boldsymbol{\gamma}_{\mathbf{z}} \dot{\mathbf{z}} \\ & + \sum_{i=1}^q g_{pi} \hat{\boldsymbol{\theta}}_i^T \boldsymbol{\Gamma}_{\theta_i}^{-1} \dot{\hat{\boldsymbol{\theta}}}_i + \sum_{i=1}^q \frac{g_{pi} \tilde{\lambda}_i \dot{\tilde{\lambda}}_i}{\boldsymbol{\Gamma}_{\lambda_i}} + \sum_{i=1}^q \frac{g_{pi} \hat{\boldsymbol{\theta}}_i \dot{\hat{\boldsymbol{\theta}}}_i}{\boldsymbol{\Gamma}_{\theta_i}} \end{aligned} \quad (44)$$

By using the Young's inequality, one can obtain Equations (46), (48), and Equations (45)–(49) would be incorporated in the further derivation.

$$\begin{aligned} \mathbf{v}_e^T \mathbf{M} \dot{\mathbf{v}}_e = & \mathbf{v}_e^T \left(\mathbf{M} \dot{\boldsymbol{\beta}}_v + \boldsymbol{\zeta} - b_v \mathcal{S}_v(v) \boldsymbol{\omega}_v - \boldsymbol{\alpha}_u + \boldsymbol{\alpha}_u \right. \\ & \left. - \mathbf{T}(\boldsymbol{\beta}) \mathbf{g}_p \mathbf{A} - \mathbf{T}(\boldsymbol{\beta}) \mathbf{g}_p \mathbf{v}_d + \mathbf{T}(\boldsymbol{\beta}) \boldsymbol{\omega}_p \right) \\ \leq & -\mathbf{v}_e^T \mathbf{k}_v \mathbf{v}_e - \mathbf{v}_e^T \mathbf{J}^T(\boldsymbol{\psi}) \boldsymbol{\eta}_e + \frac{\rho_v^2}{\lambda_{\min}\{\mathbf{k}_{vm}\}} \\ & + \frac{b_v^2 \boldsymbol{\omega}_v^T \boldsymbol{\omega}_v}{\lambda_{\min}\{\mathbf{k}_{vm}\}} + \mathbf{v}_e^T \left[(\mathbf{M} - \mathbf{I}) \dot{\boldsymbol{\beta}}_v + \boldsymbol{\alpha}_u \right. \\ & \left. - \mathbf{T}(\boldsymbol{\beta}) \mathbf{g}_p \mathbf{A} - \mathbf{T}(\boldsymbol{\beta}) \mathbf{g}_p \mathbf{v}_d + \mathbf{T}(\boldsymbol{\beta}) \boldsymbol{\omega}_p \right] \end{aligned} \quad (45)$$

$$\begin{aligned} & \chi_v^T \dot{\chi}_v + \eta_e^T J(\psi) \chi_v \\ &= \chi_v^T (-\varrho_v^{-1} \chi_v + R_v(\eta_e, \dot{\eta}_e, \psi, r)) + \|\eta_e\|^2 \\ & \quad + \frac{\|J(\psi) \chi_v\|^2}{4} \\ &= - \sum_{i=u,v,r} (-\varrho_i^{-1} \chi_i^2 + \chi_i R_i(\eta_e, \dot{\eta}_e, \psi, r)) \\ & \quad + \|\eta_e\|^2 + \frac{\|\chi_v\|^2}{4} \end{aligned} \tag{46}$$

$$\begin{aligned} & \leq - \sum_{i=u,v,r} \left[\left(\frac{1}{\varrho_i} - \frac{1}{4} - \frac{\bar{R}_i^2}{2b} \right) \chi_i^2 - \frac{b}{2} + \left(-\frac{R_i^2}{\bar{R}_i^2} \right) \frac{\chi_i^2 \bar{R}_i^2}{2b} \right] + \|\eta_e\|^2 \\ & \leq - \sum_{i=u,v,r} \left(\frac{1}{\varrho_i} - \frac{1}{4} - \frac{\bar{R}_i^2}{2b} \right) \chi_i^2 + \frac{3b}{2} + \|\eta_e\|^2 \end{aligned}$$

$$\begin{aligned} \tilde{z}^T \gamma_{\tilde{z}} \dot{\tilde{z}} &= \tilde{z}^T \gamma_{\tilde{z}} (\alpha_u - \Phi_v(\cdot) k_m v_e - \varsigma \tilde{z} - \dot{v}) \\ &= \tilde{z}^T \gamma_{\tilde{z}} \alpha_u - \Phi_v(\cdot) \tilde{z}^T \gamma_{\tilde{z}} k_m v_e - \tilde{z}^T \gamma_{\tilde{z}} \varsigma \tilde{z} \\ & \quad + \tilde{z}^T \gamma_{\tilde{z}} (\dot{\beta}_v - \dot{v}) - \tilde{z}^T \gamma_{\tilde{z}} \dot{\beta}_v \end{aligned} \tag{47}$$

$$\begin{aligned} &= \tilde{z}^T \gamma_{\tilde{z}} \left[(M - I) \dot{\beta}_v + \alpha_u - T(\beta) g_p A \right. \\ & \quad \left. - T(\beta) g_p v_d + T(\beta) \varpi_p \right] - \tilde{z}^T \gamma_{\tilde{z}} \varsigma \tilde{z} \end{aligned}$$

$$\begin{aligned} v_e^T (M - I) \dot{\beta}_v &= v_e^T (M - I) \varrho_v^{-1} \chi_v \\ & \leq \left\| (M - I) \varrho_v^{-1} \right\|_F^2 \|v_e\|^2 + \frac{1}{4} \|\chi_v\|^2 \end{aligned} \tag{48}$$

$$\begin{aligned} \omega_v^T \omega_v &= \|A_v''\| \\ &= \frac{\omega_{u,1}^T \omega_{u,1} + \omega_{u,2}^T \omega_{u,2} + \dots + \omega_{r,3}^T \omega_{r,3}}{\|A_v\|_F^2} v_e^T v_e \\ &= v_e^T v_e \end{aligned} \tag{49}$$

Incorporating Equations (45)–(49) in the calculation, it yields Equation (50), where b indicates a positive small constant for the analysis.

$$\begin{aligned} \dot{V} & \leq -(\lambda_{\min}\{k_\eta\} - 1) \eta_e^T \eta_e - \sum_{i=u,v,r} \left(\frac{1}{\varrho_i} - \frac{1}{2} - \frac{\bar{R}_i^2}{2b} \right) \chi_i^2 \\ & \quad - \left(\lambda_{\min}\{k_p\} - \left\| (M - I) \varrho_v^{-1} \right\|_F^2 - \frac{b_v^2}{\lambda_{\min}\{k_m\}} \right) v_e^T v_e \\ & \quad - \lambda_{\min}\{\gamma_{\tilde{z}} \varsigma\} \tilde{z}^T \tilde{z} + (v_e + \gamma_{\tilde{z}} \tilde{z})^T \left[\alpha_u - T(\beta) g_p A \right. \end{aligned}$$

$$\begin{aligned} & \left. - T(\beta) g_p v_d + T(\beta) \varpi_p \right] + \sum_{i=1}^q \frac{g_{pi} \tilde{\lambda}_i \dot{\lambda}_i}{\Gamma_{\lambda_i}} + \sum_{i=1}^q \frac{g_{pi} \tilde{\theta}_i \dot{\theta}_i}{\Gamma_{\theta_i}} \\ & \quad + \sum_{i=1}^q g_{pi} \tilde{\vartheta}_i^T \Gamma_{\vartheta_i}^{-1} \dot{\vartheta}_i + \frac{\rho_v^2}{\lambda_{\min}\{k_m\}} + \frac{3b}{2} \end{aligned} \tag{50}$$

Then the time derivative \dot{V} is derived as Equation (53) with Equations (38), (51), (52).

$$\begin{aligned} (v_e + \gamma_{\tilde{z}} \tilde{z})^T T(\beta) \varpi_p &= (v_e + \gamma_{\tilde{z}} \tilde{z})^T T(\beta) g_p \theta \\ &= \sum_{i=1}^q g_{pi} \theta_i \sum_{k=u,v,r} (k_e + \gamma_{\tilde{z}k} \tilde{z}_k) T_{ki}(\cdot) \\ &= \sum_{i=1}^q g_{pi} (\hat{\theta}_i - \tilde{\theta}_i) \sum_{k=u,v,r} (k_e + \gamma_{\tilde{z}k} \tilde{z}_k) T_{ki}(\cdot) \\ & \leq \sum_{i=1}^q g_{pi} \left[\hat{\theta}_i (v_e + \gamma_{\tilde{z}} \tilde{z})^T T_i(\cdot) \tanh \left(\frac{\hat{\theta}_i (v_e + \gamma_{\tilde{z}} \tilde{z})^T T_i(\cdot)}{\varepsilon} \right) \right. \\ & \quad \left. + 0.2785\varepsilon \right] - \sum_{i=1}^q g_{pi} \tilde{\theta}_i (v_e + \gamma_{\tilde{z}} \tilde{z})^T T_i(\cdot) \end{aligned} \tag{51}$$

$$\begin{aligned} (v_e + \gamma_{\tilde{z}} \tilde{z})^T \alpha_u &= (v_e + \gamma_{\tilde{z}} \tilde{z})^T T(\beta) g_p \lambda T^\dagger(\beta) \alpha_u \\ &= (v_e + \gamma_{\tilde{z}} \tilde{z})^T T(\beta) g_p (\hat{\lambda} - \tilde{\lambda}) T^\dagger(\beta) \alpha_u \\ &= - \sum_{i=1}^q g_{pi} \tilde{\lambda}_i \sum_{k=u,v,r} \sum_{j=u,v,r} T_{ij}^\dagger(\cdot) T_{ki}(\cdot) (k_e + \gamma_{\tilde{z}k} \tilde{z}_k) \alpha_{jp} \\ & \quad + (v_e + \gamma_{\tilde{z}} \tilde{z})^T T(\beta) g_p \hat{\lambda} T^\dagger(\beta) \alpha_u \end{aligned} \tag{52}$$

$$\begin{aligned} \dot{V} & \leq -(\lambda_{\min}\{k_\eta\} - 1) \eta_e^T \eta_e - \sum_{i=u,v,r} \left(\frac{1}{\varrho_i} - \frac{1}{2} - \frac{\bar{R}_i^2}{2b} \right) \chi_i^2 \\ & \quad - \left(\lambda_{\min}\{k_p\} - \left\| (M - I) \varrho_v^{-1} \right\|_F^2 - \frac{b_v^2}{\lambda_{\min}\{k_m\}} \right) v_e^T v_e \\ & \quad - \lambda_{\min}\{\gamma_{\tilde{z}} \varsigma\} \tilde{z}^T \tilde{z} - \sum_{i=1}^q g_{pi} \tilde{\theta}_i (v_e + \gamma_{\tilde{z}} \tilde{z})^T T_i(\cdot) \\ & \quad - \sum_{i=1}^q g_{pi} \tilde{\lambda}_i \sum_{k=u,v,r} \sum_{j=u,v,r} T_{ij}^\dagger(\cdot) T_{ki}(\cdot) (k_e + \gamma_{\tilde{z}k} \tilde{z}_k) \alpha_{jp} \\ & \quad + \sum_{i=1}^q \frac{g_{pi} \tilde{\lambda}_i \dot{\lambda}_i}{\Gamma_{\lambda_i}} + \sum_{i=1}^q \frac{g_{pi} \tilde{\theta}_i \dot{\theta}_i}{\Gamma_{\theta_i}} + \sum_{i=1}^q g_{pi} \tilde{\vartheta}_i^T \Gamma_{\vartheta_i}^{-1} \dot{\vartheta}_i \\ & \quad + \frac{\rho_v^2}{\lambda_{\min}\{k_m\}} + \frac{3b}{2} \end{aligned} \tag{53}$$

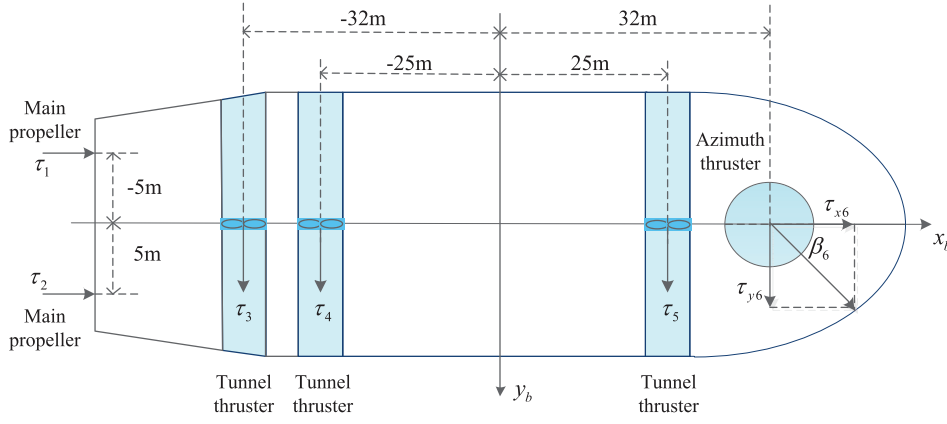


FIGURE 3 Thruster configuration diagram of the supply marine vehicle

Submitting Equations (40)–(42) into Equation (53), one could obtain Equation (54),

$$\begin{aligned} \dot{V} \leq & -(\lambda_{\min}\{\mathbf{k}_\eta\} - 1)\boldsymbol{\eta}_e^T \boldsymbol{\eta}_e - \sum_{i=u,v,r} \left(\frac{1}{\varrho_i} - \frac{1}{2} - \frac{\bar{R}_i^2}{2b} \right) \chi_i^2 \\ & - \left(\lambda_{\min}\{\mathbf{k}_v\} - \left\| (\mathbf{M} - \mathbf{I})\boldsymbol{\varrho}_v^{-1} \right\|_F^2 - \frac{b_v^2}{\lambda_{\min}\{\mathbf{k}_{v1}\}} \right) \mathbf{v}_e^T \mathbf{v}_e \\ & - \lambda_{\min}\{\boldsymbol{\gamma}_\zeta \boldsymbol{\zeta}\} \boldsymbol{\zeta}^T \boldsymbol{\zeta} - \sum_{i=1}^q \frac{\sigma_{\vartheta_i} \inf\{g_{\vartheta_i}\} \tilde{\boldsymbol{\vartheta}}_i^T \tilde{\boldsymbol{\vartheta}}_i}{2} \\ & - \sum_{i=1}^q \frac{\sigma_{\lambda_i} \inf\{g_{\lambda_i}\} \tilde{\lambda}_i^2}{2} - \sum_{i=1}^q \frac{\sigma_{\theta_i} \inf\{g_{\theta_i}\} \tilde{\theta}_i^2}{2} + \Delta \end{aligned} \quad (54)$$

where $\Delta = \rho_v^2 / \lambda_{\min}\{\mathbf{k}_{v1}\} + 3b/2 + \sum_{i=1}^q 0.2785\epsilon \sup\{g_{\vartheta_i}\} + \sum_{i=1}^q \sup\{g_{\lambda_i}\}((\sigma_{\lambda_i}/2)(\lambda_i - \hat{\lambda}_i(0))^2 + (\sigma_{\theta_i}/2)(\theta_i - \hat{\theta}_i(0))^2 + (\sigma_{\vartheta_i}/2)(\vartheta_i - \hat{\vartheta}_i(0))^T(\vartheta_i - \hat{\vartheta}_i(0)))$.

Furthermore, Equation (54) could be further derived as Equation (55) with $a = \min\{(\lambda_{\min}\{\mathbf{k}_\eta\} - 1), (\sum_{i=u,v,r} (1/\varrho_i - 1/2 - \bar{R}_i^2/2b)), (\lambda_{\min}\{\mathbf{k}_v\} - 1/\lambda_{\min}\{\mathbf{k}_{v1}\} - \left\| (\mathbf{M} - \mathbf{I})\boldsymbol{\varrho}_v^{-1} \right\|_F^2), \lambda_{\min}\{\boldsymbol{\gamma}_\zeta \boldsymbol{\zeta}\}, (\sigma_{\lambda_1} \Gamma_{\lambda_1}/2), \dots, (\sigma_{\lambda_q} \Gamma_{\lambda_q}/2), (\sigma_{\theta_1} \Gamma_{\theta_1}/2), \dots, (\sigma_{\theta_q} \Gamma_{\theta_q}/2)\}$.

$$\dot{V} \leq -2aV + \Delta \quad (55)$$

By integrating Equation (55), one could obtain that $V(t) \leq (V(0) - (\Delta/2a)) \exp(-2at) + (\Delta/2a)$. By fusion of the closed-loop gain shaping algorithm [29], $V(t)$ could converge to $\Delta/2a$ with $t \rightarrow \infty$, and the term Δ is able to achieve small enough by tuning the designed parameters. Thus, all the error variables of the closed-loop system are SGUUB under the proposed control scheme. \square

5 | NUMERICAL SIMULATIONS

To verify and evaluate the effectiveness and merits of the proposed algorithm, the numerical simulations, including the

TABLE 1 Model parameters

Items	Value	Items	Value
X_i	-0.7212×10^6	Y_i	-3.6921×10^6
Y_r	-1.0234×10^6	$I_\zeta - N_r$	3.7454×10^9
X_u	5.0242×10^4	Y_v	2.7229×10^5
Y_r	-4.3933×10^6	$Y_{ v }$	1.7860×10^4
$X_{ u }$	1.0179×10^3	$Y_{ r }$	-3.0068×10^5
N_v	-4.3821×10^6	N_r	4.1894×10^8
$N_{ v }$	-2.4684×10^5	$N_{ r }$	6.5759×10^6

comparative experiment and the experiment with dead-zone constraints and actuator faults, are provided in this section. For this purpose, one consider the supply marine vehicle (length of 76.2 m, mass of 4.591×10^6 kg) as the plant. Figure 3 shows thruster configuration for the supply marine vehicle. The model parameters for the plant are provided in Table 1.

The environment disturbances are simulated by fusion of the physical-based mathematical model, that is the JONSWAP wave spectrums and the NORSOK wind spectrums are employed to generate the wind-generated wave and sea wind, respectively. As for the model, the detailed descriptions have been provided in [30]. Figure 4 shows the two-dimensional (2-D) wind field and the corresponding wind-generated waves with the mean wind speed $V_{wind} = 16.3$ m/s and wind direction $\psi_{wind} = 90$ deg. And the simulated environment disturbances would be applied to the numerical simulations.

5.1 | Comparative experiment

In this section, the proposed algorithm will be compared with the one in [8] considering dead-zone input to illustrate the superiority of the dead-zone compensation mechanism. In this experiment, the desired attitude is $\boldsymbol{\eta}_d = [10 \text{ m}, 10 \text{ m}, 120 \text{ deg}]^T$. The initial states of the DP vehicle are $[x(0), y(0), \psi(0), u(0), v(0), r(0)] = [0 \text{ m}, 0 \text{ m}, 135 \text{ deg}, 0 \text{ m/s}, 0 \text{ m/s}, 0 \text{ deg/s}]$ and the corresponding design parameters are shown in Equation (56). The extending operation discussed in Remark 2 is required since

the supply marine vehicle is equipped with a rotatable thruster. So the design parameters $\Gamma_\lambda, \Gamma_\theta, \sigma_\lambda, \sigma_\theta$ consist of seven elements. In addition, the RBF NNs for $F_{mn}(v)$ contain 25 nodes and its centres spaced of u, v, r are $[-2.5 \text{ m/s}, 2.5 \text{ m/s}], [-2.5 \text{ m/s}, 2.5 \text{ m/s}]$ and $[-0.6 \text{ rad/s}, 0.6 \text{ rad/s}]$, respectively.

$$\begin{aligned} \Gamma_\lambda &= [0.7, 0.7, 0.3, 0.1, 0.2, 0.4, 0.3]^T, \mathbf{k}_\eta = \text{diag}\{0.3, 0.3, 0.1\}, \\ \Gamma_\theta &= [0.6, 0.5, 0.5, 0.2, 0.4, 0.1, 0.4]^T, \mathbf{k}_\nu = \text{diag}\{0.2, 0.2, 5.5\}, \\ \sigma_\lambda &= [4.2, 4.2, 6.3, 4.8, 4.2, 5.5, 7.6]^T, s_r = 1.8, s_l = 2.8, \\ \sigma_\theta &= [4.5, 4.6, 5.3, 3.9, 5.6, 6.7, 5.8]^T, b_r = 0.8, b_l = -0.55, \\ \mathbf{k}_{mn} &= \text{diag}\{0.3, 0.072, 0.78\}, \boldsymbol{\zeta} = \text{diag}\{0.9, 1.5, 0.9\}, \\ \boldsymbol{\varrho}_v &= \text{diag}\{0.01, 0.01, 0.01\}, \boldsymbol{\gamma}_\zeta = \text{diag}\{0.24, 0.4, 0.24\}, \end{aligned} \quad (56)$$

Remark 4. The parameter settings in numerical simulations are tuned on the basis of the trial and error strategy. Taking the control parameter as an example, the large gain coefficient can ensure the control performance of the plant. However, that might give rise to the unexpected large control signals, which would cause the actuator input exceed the constraint. Therefore, in the process of parameters adjustment, the parameters $\mathbf{k}_\eta, \mathbf{k}_\nu, \dots, \mathbf{k}_{mn}$ should be set as a large value respectively. Subsequently, one can decrease these parameters gradually to obtain the satisfying system performance under the actuator input constraint by testing the simulation runs. Other parameter settings are similar to the above parameter selection method, which needs no further elaboration here.

$$\begin{aligned} MSE &= \frac{1}{t_\infty - t_0} \int_{t_0}^{t_\infty} |e(t)|^2 dt \\ MAE &= \frac{1}{t_\infty - t_0} \int_{t_0}^{t_\infty} |u(t)| dt \end{aligned} \quad (57)$$

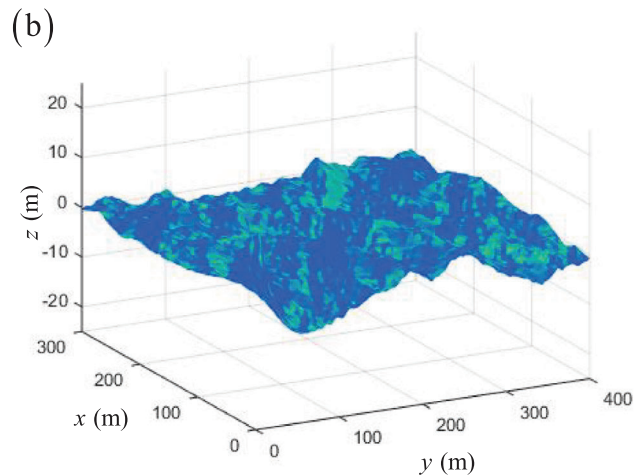
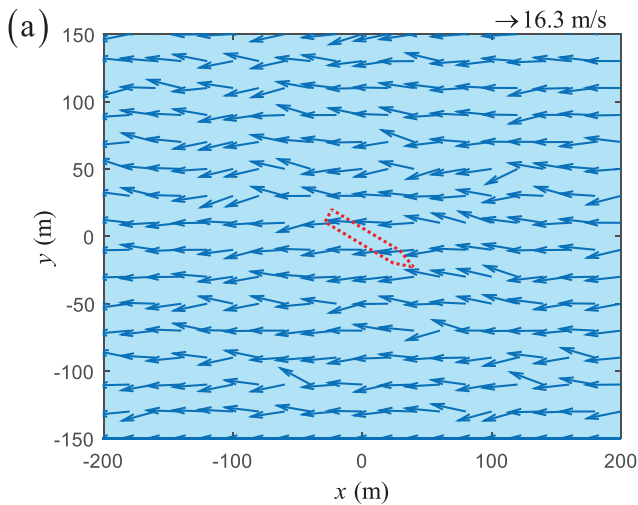


FIGURE 4 Environment disturbances: (a) 2-D wind field. (b) The corresponding wind-generated waves

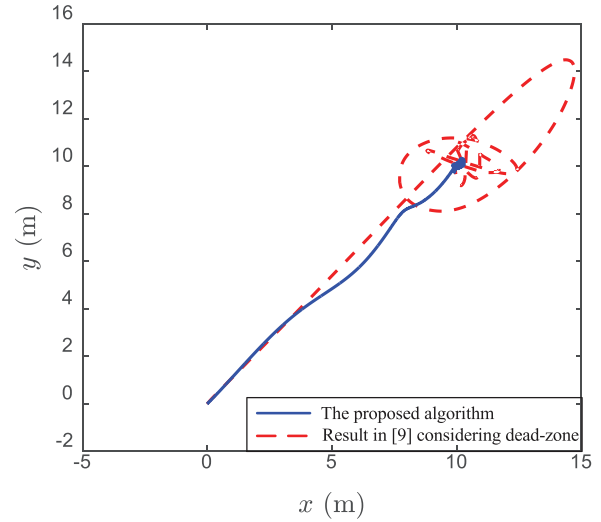


FIGURE 5 Comparison of the dynamic positioning control trajectory

$$MAE = \frac{1}{t_\infty - t_0} \int_{t_0}^{t_\infty} |u(t+1) - u(t)| dt$$

The corresponding comparative results are shown in Figures 5–7. Based on these results, one can conclude that the proposed algorithm is with more superior control performance compared with the results in [8]. Figure 8 shows the estimation error for the velocity variables. It is easy to see that the estimation error can converge approximately to 0 under the marine environment disturbance. That proves a fact that the estimator is with good prediction performance. And Figure 9 shows the curves of the estimation for dead-zone parameters. It is not hard to see that the proposed algorithm is with great parameter estimation performance for the dead-zone. To further evaluate the both algorithms, one employ three performance specifications (57) for the quantitative analysis, that is the mean square error (*MSE*), the mean absolute control effort (*MAE*), the mean total variation (*MTV*) of the control. *MSE* is utilized to measure the

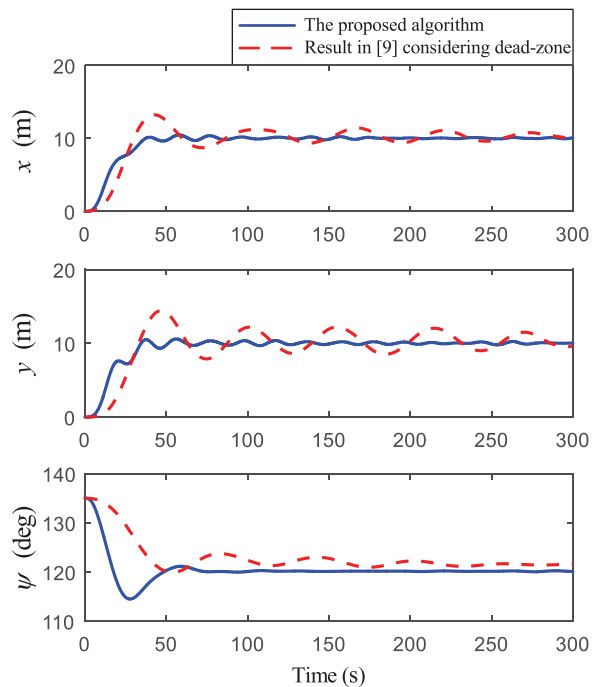


FIGURE 6 Comparison of the attitude variables x, y, ψ

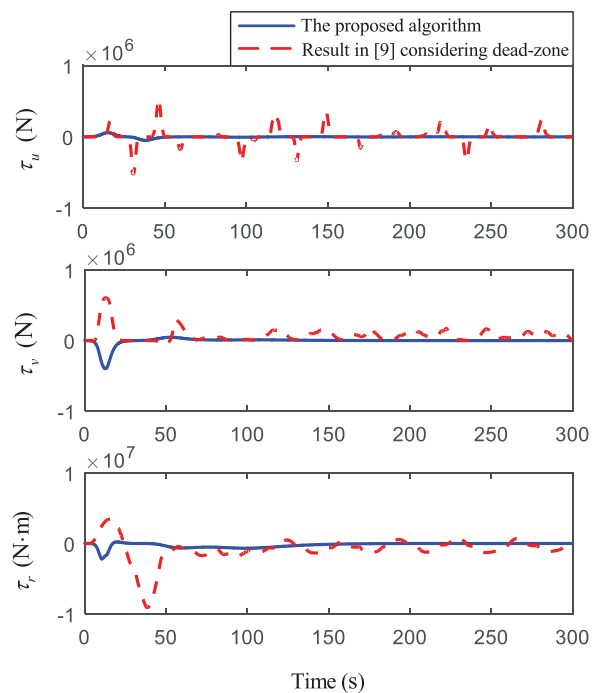


FIGURE 7 Comparison of the control efforts τ_u, τ_v, τ_r

response performance, and smaller MAE and MTV denote less energy consumption and better smoothness property respectively. The corresponding quantitative results are provided in Table 2. Based on the quantitative analysis, one could conclude that the proposed algorithm is with better servo and regulatory

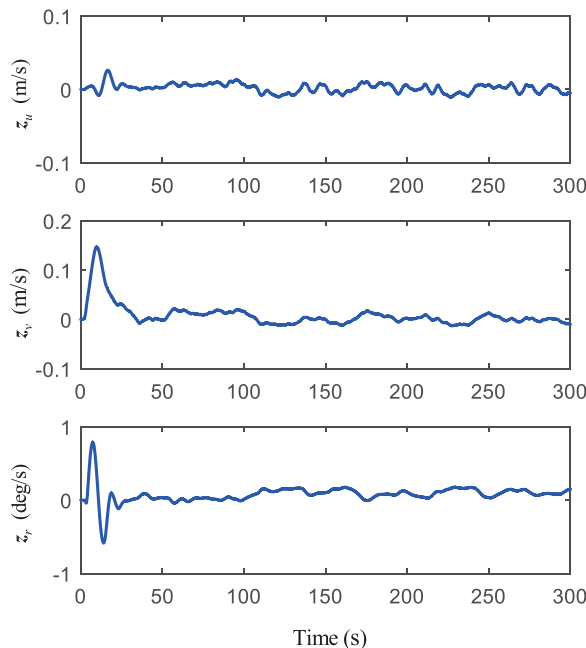


FIGURE 8 The estimation errors z_u, z_v, z_r for the velocity variables u, v, r

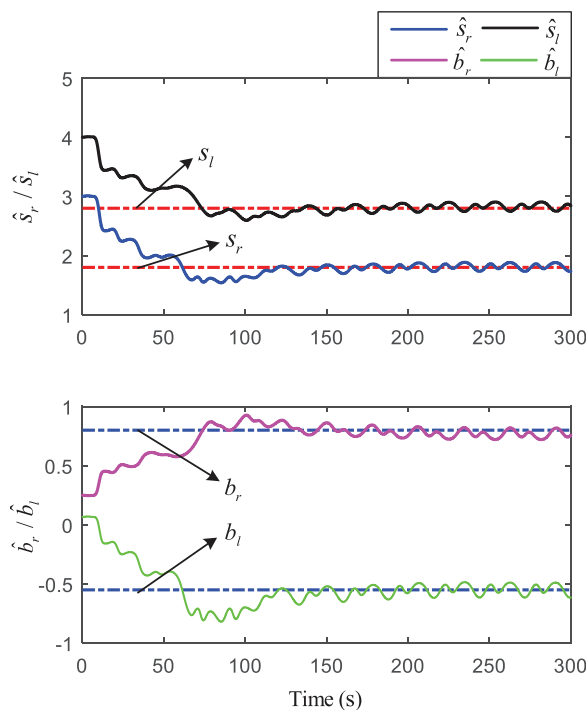


FIGURE 9 The estimation of dead-zone parameters

performance and less energy consumption. In addition, the held computer memory (MH) is employed to evaluate the computing burden for the both algorithms, and the comparative results are given in Table 3. The results imply that the proposed algorithm has the superiority in simplifying computation.

TABLE 2 Quantitative comparison of performances for the proposed algorithm and the one in [8] considering dead-zone

Indexes	Items	The proposed algorithm	The algorithm in [8] considering dead-zone
MSE	x_e (m)	1.9863	4.8498
	y_e (m)	2.9342	7.8481
	ψ_e (deg)	0.7785	5.5464
	τ_u (N)	4.7467×10^3	3.7844×10^4
MAE	τ_v (N)	1.6097×10^4	5.1489×10^4
	τ_r (N · m)	2.2042×10^5	7.7945×10^5
	τ_u (N)	8.7401	70.8486
MTV	τ_v (N)	30.1550	48.4644
	τ_r (N · m)	220.9221	1587.8164

TABLE 3 Comparison of the computation load for the proposed algorithm and the one in [8] considering dead-zone

Indexes	IPC type	The proposed algorithm	The algorithm in [8] considering dead-zone
MH	CPU (<i>i7</i> – 4710)	364, 685 KB	464, 787 KB
	2.70 GHz		
MH	CPU (<i>i5</i> – 7200U)	566, 824 KB	721, 355 KB
	2.50 GHz		
MH	CPU (<i>J1900</i>)	635, 354 KB	785, 278 KB
	1.99 GHz		

5.2 | Experiment with actuator faults

In this section, an experiment is provided to verify the effectiveness of the fault compensation mechanism under the dead-zone constraints. For this purpose, all thrusters and propellers are chosen as the actuators with a dead-zone constraints, and the dead-zone parameters are consistent with those parameters in the comparative experiment. Figure 10 shows the ship motion trajectory under dead-zone constraints and actuator faults, where the initial attitude is $\eta = [0 \text{ m}, 6 \text{ m}, 136 \text{ deg}]^T$, the desired attitude is $\eta_{d1} = [10 \text{ m}, 24 \text{ m}, 120 \text{ deg}]^T$ during the time $t \in [0, 500]$, the desired attitude is $\eta_{d2} = [16 \text{ m}, 0 \text{ m}, 140 \text{ deg}]^T$ during the time $t \in (500, 1000]$, and the desired attitude is $\eta_{d3} = [8 \text{ m}, -40 \text{ m}, 160 \text{ deg}]^T$ during the time $t \in (1000, 1500]$. Note that the vessels in Figure 9 only denote the heading stabilizing at corresponding desired attitude. Furthermore, a bias fault ($k_{p5} = 1$, $\epsilon_5 = 0.1$) is set at 800s for NO.5 actuator, and the PLOE fault ($k_{p3} = 0.3$, $\epsilon_3 = 0$) and bias fault ($k_{p1} = 1$, $\epsilon_1 = 0.2$) are simultaneously set at 1300s for NO.3 and NO.1 actuator respectively. And the corresponding curves are shown in Figures 10 and 11 under the proposed compensation scheme. The curves of control input p_i as well as β_6 are provided in Figure 10, it is easy to see that the dead-zone constraints and actuator faults are compensated successfully from the these curves. The controller is able to compensate dead-zone con-

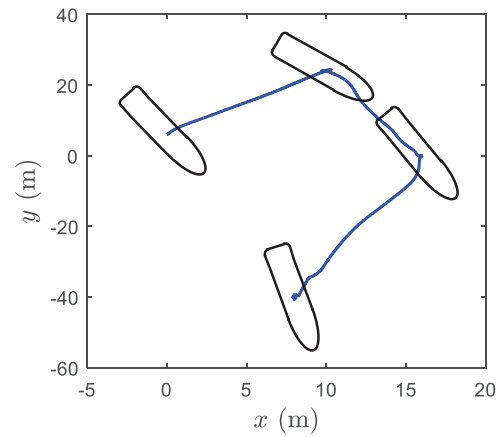


FIGURE 10 The ship motion trajectory with dead-zone constraints and actuator faults

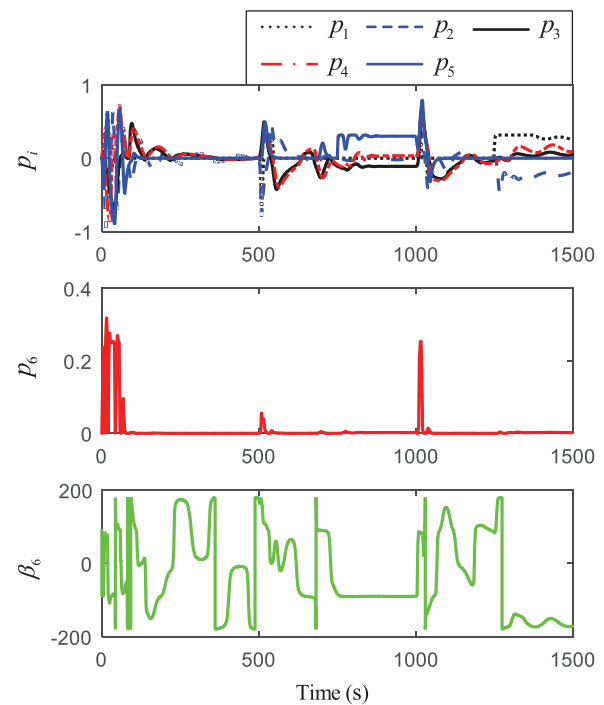


FIGURE 11 Actual control inputs with dead-zone constraints and actuator faults

straints and actuator faults by properly allocating the input to each actuator. Moreover, the curve of β_6 occurs jumping phenomenon in Figure 11, which does not seem to be satisfactory. But that's not the case. Actually, the range of the bearing angle β_6 is $(-180 \text{ deg}, 180 \text{ deg}]$, and there exist a transforming operation for the rotatable thruster in practical engineering. So the curve is smooth and reasonable. The composite adaptive laws associated with gain and fault are shown in Figure 12, they have the ability to compensate the unknown gain uncertainties and actuator faults by updating themselves online.

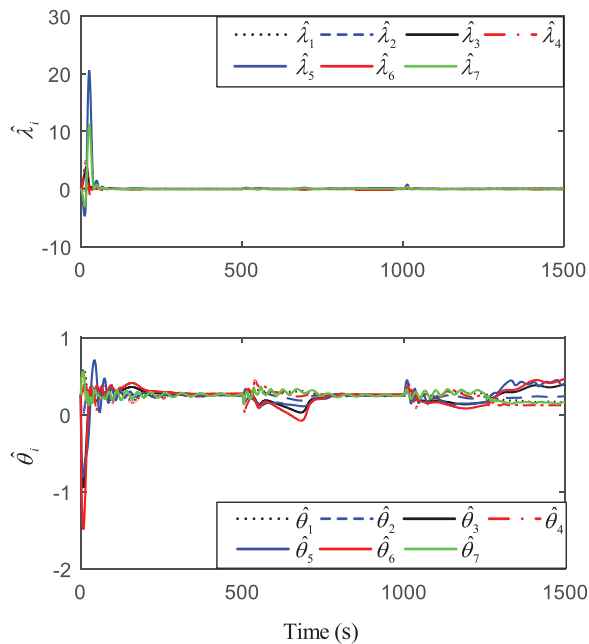


FIGURE 12 Composite adaptive law $\hat{\lambda}_i$ and $\hat{\theta}_i$ with dead-zone constraints and actuator faults

6 | CONCLUSION

This paper presents a composite adaptive DP control algorithm in the presence of the dead-zone non-linearities and actuator faults by virtue of the DSC, NNs and robust neural damping technique. The composite intelligent learning methodology is applied to the DP vehicle to improve the control performance and compensation accuracy. Furthermore, the adaptive smooth inverse function is employed in dead-zone model to compensate the dead-zone non-linearity. Only two adaptive parameters are required to release the constraints of gain uncertainty and actuator faults for each actuator. The effectiveness of the proposed algorithm is verified by the comparative experiment and the experiment with actuator faults. In the comparative experiment, the compared algorithm is added the dead-zone constraints to illustrate the validity of the proposed compensation scheme.

Note, this work cannot attend to every detail of the control design, for example the uncertainty and imprecision of the dead-zone parameters in practical applications, non-linear dynamics in the actuator. That would be the further problem to be solved in the following works.

ACKNOWLEDGEMENTS

The paper is partially supported by the National Natural Science Foundation of China (No. 51909018), the Natural Science Foundation of Liaoning Province (No. 20170520189, 20180520039), the Science and Technology Innovation Foundation of Dalian City (No. 2019J12GX026) and the Fundamental Research Funds for the Central Universities (NO. 3132021132, 3132021340). The authors would like to thank anonymous reviewers for their valuable comments.

ORCID

Guoqing Zhang  <https://orcid.org/0000-0002-7774-5444>

REFERENCES

- Lin, X., et al.: Nonlinear adaptive fuzzy output-feedback controller design for dynamic positioning system of ships. *Ocean Eng.* 158(4), 186–195 (2018)
- Du, J., et al.: A robust adaptive neural networks controller for maritime dynamic positioning system. *Neurocomputing* 110, 128–136 (2013)
- Xia, G., et al.: Adaptive neural network controller applied to dynamic positioning of a remotely operated vehicle. In: 2013 MTS/IEEE OCEANS, Bergen (2013)
- Xu, B., Shi, Z., Yang, C.: Composite neural dynamic surface control of a class of uncertain nonlinear systems in strict-feedback form. *IEEE Trans. Cybern.* 44(12), 2626–2634 (2014)
- Xu, B., Sun, F.: Composite intelligent learning control of strict-feedback systems with disturbance. *IEEE Trans. Cybern.* 48(2), 730–741 (2018)
- Zhang, G., et al.: Improved composite learning path-following control for the underactuated cable-laying ship via the double layers logical guidance. *Ocean Eng.* 207, 107342 (2020)
- Louei-pour, M., et al.: Wave Filtering and State Estimation in Dynamic Positioning of Marine Vessels Using Position Measurement. *IEEE Trans. Instrum. Meas.* 64(12), 3253–3261 (2015)
- Morishita, H.M., Souza, C.E.S.: Modified observer backstepping controller for a dynamic positioning system. *Control Eng. Pract.* 33, 105–114 (2014)
- Liang, K., et al.: Adaptive sliding mode output feedback control for dynamic positioning ships with input saturation. *Ocean Eng.* 206, 107245 (2020)
- Peng, Z., Wang, D., Wang, J.: Cooperative dynamic positioning of multiple marine offshore vessels: A modular design. *IEEE/ASME Trans. Mechatron.* 21(3), 1210–1221 (2016)
- Deng, W., Yao, J., Ma, D.: Robust adaptive precision motion control of hydraulic actuators with valve dead-zone compensation. *ISA Trans.* 70, 269–278 (2017)
- Liu, Z., et al.: Adaptive tracking control for a class of nonlinear systems with a fuzzy dead-zone input. *IEEE Trans. Fuzzy Syst.* 23(1), 193–204 (2015)
- Jia, X., et al.: Adaptive output feedback tracking of nonlinear systems with uncertain nonsymmetric dead-zone input. *ISA Trans.* 95, 48–54 (2019)
- Badihi, H., Zhang, Y., Hong, H.: Wind turbine fault diagnosis and fault-tolerant torque load control against actuator faults. *IEEE Trans. Control Syst. Technol.* 23(4), 1351–1372 (2015)
- Moradi, M., Fekih, A.: A stability guaranteed robust fault tolerant control design for vehicle suspension systems subject to actuator faults and disturbances. *IEEE Trans. Control Syst. Technol.* 23(3), 1164–1171 (2015)
- Zhang, G., et al.: Active fault-tolerant control for electric vehicles with independently driven rear in-wheel motors against certain actuator faults. *IEEE Trans. Control Syst. Technol.* 24(5), 1557–1572 (2016)
- Dong, J., Yang, G.: Reliable state feedback control of T-S fuzzy systems with sensor faults. *IEEE Trans. Fuzzy Syst.* 23(2), 421–433 (2015)
- Gao, Z.: Fault estimation and fault-tolerant control for discrete-time dynamic systems. *IEEE Trans. Ind. Electron.* 62(6), 3874–3884 (2015)
- Shen, Q., et al.: Active fault-tolerant control system design for spacecraft attitude maneuvers with actuator saturation and faults. *IEEE Trans. Ind. Electron.* 66(5), 3763–3772 (2019)
- Du, J., et al.: A robust adaptive neural networks controller for maritime dynamic positioning system. *Neurocomputing* 110, 128–136 (2013)
- Hu, X., Du, J., Sun, Y.: Robust adaptive control for dynamic positioning of ships. *IEEE J. Oceanic Eng.* 42(4), 826–835 (2017)
- Fossen, T.I.: *Handbook of Marine Craft Hydrodynamics and Motion Control*. Wiley, New York (2011)
- Fossen, T.I., Strand, J.: Nonlinear passive weather optimal positioning control (WOPC) system for ship and rigs: Experimental results. *Int. J. Control* 74, 1435–1446 (2011)
- Xing, L., et al.: Adaptive compensation for actuator failures with event-triggered input. *Automatica* 85, 129–136 (2017)

25. Wang, C., Wen, C., Lin, Y.: Adaptive actuator failure compensation for a class of nonlinear systems with unknown control direction. *IEEE Trans. Autom. Control* 62(1), 385–392 (2017)
26. Su, X., et al.: Direct adaptive compensation for actuator failures and dead-zone constraints in tracking control of uncertain nonlinear systems. *Inf. Sci.* 417, 328–343 (2017)
27. Zhang, G., et al.: Robust neural event-triggered control for dynamic positioning ships with actuator faults. *Ocean Eng.* 207, 107292 (2020)
28. Xu, B., et al.: Online recorded data-based composite neural control of strict-feedback systems with application to hypersonic flight dynamics. *IEEE Trans. Neural Netw. Learning Syst.* 29(8), 3839–3849 (2018)
29. Zhang, G., Zhang, X., Guan, W.: Stability analysis and design of integrating unstable delay processes using the mirror-mapping technique. *J. Process Control* 24(7), 1038–1045 (2014)
30. Aasgeir, J. Sørensen: *Marine Control Systems. Propulsion and Motion Control of Ships and Ocean Structures (Lecture Notes)*. Norwegian University of Science and Technology, Trondheim (2013)

How to cite this article: Zhang, G., et al. Improved composite adaptive fault-tolerant control for dynamic positioning vehicle subject to the dead-zone nonlinearity. *IET Control Theory Appl.* 15, 2067–2080 (2021). <https://doi.org/10.1049/cth2.12176>